# Space radiation environment effects on X-ray CCD background

# Space radiation environment effects on X-ray CCD background

David J. Hall [a,*] Andrew Holland [a]

[a] *Planetary and Space Sciences Research Institute, Open University, Walton Hall, Milton Keynes MK7 6AA, UK*

**Abstract**

Charge coupled devices (CCDs) are often employed as the detector of choice for observing X-rays in space. The instrument background experienced in orbit has a major impact on the overall sensitivity of the camera system. The instrument background for the European Space Agency X-ray Multi Mirror (XMM-Newton) mission was found to be much greater in orbit than that originally predicted pre-launch, the reasons for which still being up for discussion. The Geant4 toolkit provides a framework for Monte Carlo simulations in a variety of areas in science and is used here to simulate the instrument background for several CCD based detectors in-orbit in order to gain a further insight into the formation of the instrument background continuum. The missions discussed in this paper include the ESA XMM-Newton mission, the NASA Swift mission and the Japanese Space Agency Suzaku mission. These three missions allow a comparison between the effects of both the mission orbit and the detector construction on the instrument background count-rate. Analysis of the results from the simulation lead to the conclusion that knock-on electrons, produced when protons pass through the shielding, dominate the instrument background continuum at the XMM-Newton Highly Elliptical Orbit (HEO) with a perigee and apogee of approximately 7 000 km and 120 000 km respectively, forming an additional background component not considered in the pre-launch study. The surface properties of the detector and shielding have the greatest impact on the level of the instrument background due to the interaction length of the knock-on electrons produced. At the Low Earth Orbit (LEO) of Swift and Suzaku at approximately 600 km, the impact of the knock-on electrons is reduced due to the differing in-flux of protons, and the form of the instrument background can vary greatly with the detector construction. The inconsistencies between this study and the pre-launch simulations are discussed. Sensitivity considerations regarding the instrument background are deliberated with a view towards future missions.

*Key words:* Instrument background, XMM, Suzaku, Swift, XEUS/IXO, Geant4, CCD X-ray spectrometer, sensitivity

## 1. Introduction

The instrument background for the XMM-Newton mission was found to exceed that predicted before launch [1]. For the XMM-Newton mission, the instrument background in-orbit was found to be almost two orders of magnitude higher than was predicted pre-launch.

By using a Geant4 based Monte Carlo method it is possible to define a geometrical and physical model of the system which can then be bombarded with a suitable spectrum of particles. The geometrical model is defined by the detectors and surrounding spacecraft material used in the mission. The physical model should be consistent across all missions with the interactions of particles with matter. The difficulties thus far are only those involved with the decisions on how to best approximate the system to optimise the implementation and running time of the simulation without adversely affecting the accuracy of the results through inaccurate assumptions.

Whereas it is simply a matter of cost to replicate the detector and physical surroundings for ground based testing, it is very difficult, if not impossible, to accurately replicate the spectrum of particles incident on the detector as would be found in space. One of the main problems encountered when attempting to simulate the instrument background experienced in-orbit is due to the complexity of the spectrum of the incident particles. These particles vary with the orbit of the mission and, although the spectrum of cosmic-rays incident on any space mission can be predicted, it has to be noted that the models available are themselves not fully accurate due to the limited data sets available.

The simulations detailed here are based around a simple framework. The initial raw data is taken from a Monte Carlo based simulation written to utilise the abilities of the Geant4 toolkit. This raw data is then analysed using a selection of in-house code. The results from this analysis provide the basic framework for this paper; the consistency

* Corresponding author.
*Email address:* d.j.hall@open.ac.uk (David J. Hall).

between results for the different missions allows more general conclusions to be made. The detector construction is generally optimised towards detection efficiency (quantum efficiency), but the results of this simulation indicate that optimising the quantum efficiency for X-ray photons may come at the expense of an increase in instrument background and loss in sensitivity for the system as a whole.

## 2. Instrument background

The X-ray-like background of a CCD in space is composed of two main components: the Cosmic X-ray Background (CXB) and the instrument background. The CXB background dominates below approximately 2 keV for XMM-Newton, with the instrument background dominating at higher energies. Through the use of observations from outside the field of view, or through the observation of the night Earth at LEO, the CXB can be excluded with the instrument background remaining.

The second component, that which dominates at higher energies, is the instrument background, or the 'quiescent non X-ray background' [2]. This is the component of the background that is discussed here. The instrument background considered here is particle-induced and is mostly due to the interaction of high-energy particles with the detector surroundings. Some of the background is therefore due to secondary particles, produced when the incident particle interacts with the material surrounding the detector, and some due to unrejected minimally ionising particle tracks. The instrument background is dependent on factors such as the design of the detector housing, the camera shielding materials and the camera construction itself, and as such can be reduced through design considerations.

## 3. Mission information

### 3.1. *The ESA X-ray Multi Mirror (XMM-Newton) mission*

The XMM-Newton spacecraft contains, amongst other apparatus, the European Photon Imaging Camera (EPIC), consisting of two Metal Oxide Semi-conductor (MOS) CCD cameras [3] and one pn-CCD [4]. The pn-CCD is subject to an unobstructed beam of X-rays in normal operation, whilst the MOS cameras are placed behind the X-ray telescopes where the gratings of the Reflection Grating Spectrometer (RGS) divert approximately 50% of the incident flux to the CCDs [5]. This does not significantly affect the instrument background, as the instrument background is due to particles external to the main beam interacting with the detector surroundings and the CCD itself.

Each MOS camera consists of seven e2v technologies type 22 front-illuminated (FI) CCDs [3]. The central CCD is set at the focal point with the outer six CCDs stepped upwards by 4.5 mm in order to better follow the curvature of the focal plane. Each CCD image section consists of 600×600 square pixels of 40 µm width. The energy range of the device (with suitably high quantum efficiency) is from approximately 0.2 keV to 10 keV, and this is therefore the range of energy considered in the simulation. In order to increase the quantum efficiency for X-rays below 1 keV the pixel structure is partially etched away to leave open 40% of the electrode structure. Although the CCDs have an epitaxial layer thickness of 80 µm, the mean depleted region of the CCDs is approximately 35-40 µm [3]. The thickness of the device is found in this study to have a minimal effect on the instrument background at HEO.

The pn-CCD camera consists of 12 pn-CCDs on a single wafer, each containing 200×64 pixels of width 150 µm per CCD. The device uses a fully depleted 280 µm layer of silicon with a useful energy range of 0.15 keV to 15 keV and an open front-face [4].

To determine which events are to be accepted as X-ray like, a grading system is used. The detected events are separated as single pixel events or all X-ray like events for analysis here.

The XMM-Newton MOS instrument background spectra used for this analysis were supplied by Andrew Read, University of Leicester, Figure 1, from readily available data [6]. The MOS quiescent internal background spectrum was taken for the out of field of view sky data over an area of approximately 11 $cm^2$. The instrument background for the MOS and pn-CCD can be isolated from the total background through the use of the out of field of view (FOV) data where the CXB contribution is not present. The intensity of the instrument background component during any given observation is within approximately 10% of the mean level [7]. The instrument background spectrum for the pn-CCD was taken from [8], again with measures taken to isolate the instrument background, here through closed observations in full frame mode. The data was taken over the first three years of the mission, and as such, the variations in protron flux (and the direction and influence of the South Atlantic Anomaly, SAA) with the orbital position will be averaged over this period. The data taken for the direct comparison of the MOS and pn-CCD cameras was selected for only single pixel X-ray events and normalised. The instrument background for the pn-CCD is seen to be approximately three times greater than that for the MOS camera, Figure 3.

### 3.2. *The NASA Swift mission*

The NASA run Swift mission was launched on the 20th of November 2004. The mission was designed as a multi-wavelength observatory to observe the optical, ultraviolet, X-ray and gamma-ray emissions from Gamma Ray Bursts (GRBs) and their afterglows [9].

The X-ray Telescope on board this mission was chosen to examine the afterglow of GRBs and, as such, was required to be used in the 0.2-10 keV range. The detector used is a single MOS CCD of the same type as used in the XMM-Newton mission (the e2v CCD22). The mission has a low-

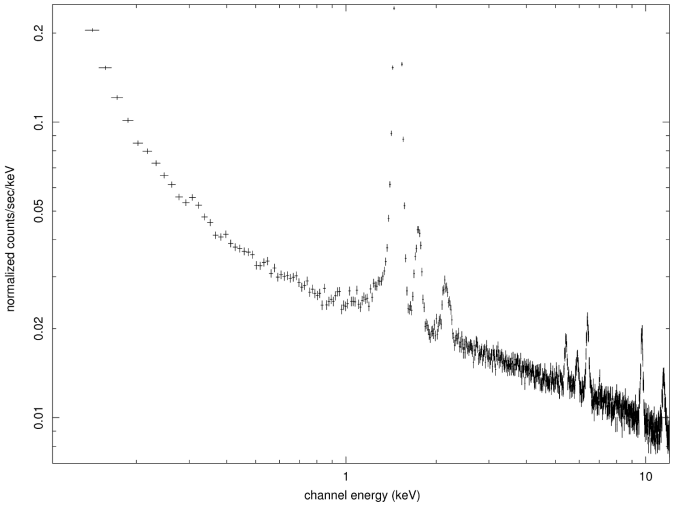


Fig. 1. The XMM-Newton MOS CCD instrument background ,taken over the out-of-FOV regions of the CCD array through removing the circular FOV region and any anomalous areas - total area of approximately 11 $cm^2$.

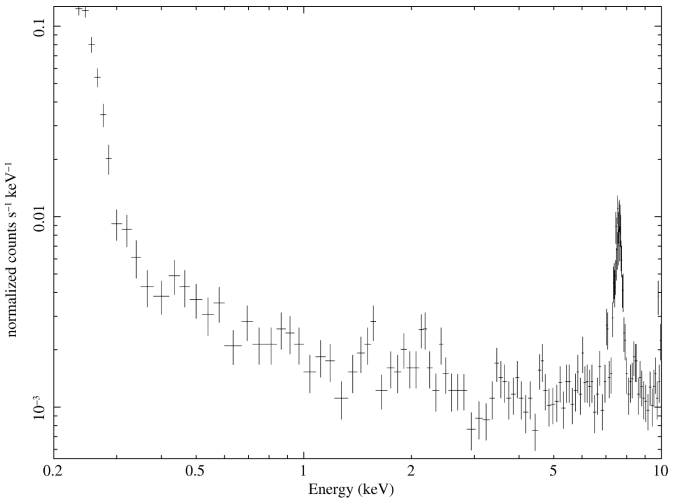


Fig. 2. The instrument background for the Swift MOS CCD (taken with the shutter closed over an area of 1.94 $cm^2$)

earth orbit, similar to that of the Japanese Space Agency Suzaku mission. The instrument background from the MOS CCD can be compared between the XMM-Newton and Swift missions to isolate the dependency on orbit.

The instrument background for the Swift MOS camera was supplied by Claudio Pagani, Penn-State University, Figure 2. The dataset was collected in September 2007 when one of the 3 dual-gyro modules exhibited anomalous behaviour, causing a loss in pointing accuracy. During this incident, Swift pointed too close to the sun and the shutter was closed. The dataset used for analysis was that taken during this period in order to isolate the instrument background. The instrument background for the Swift MOS camera has been selected for all X-ray grade events and is seen to be approximately three to four times lower than that for the XMM-Newton MOS camera, comparing the spectra for all X-ray grade events. For comparison between the MOS cameras on the Swift and XMM-Newton missions, all X-ray-like events were selected due to the ready availability of this data for the Swift mission. The data collected over the period in September 2007 is consistent ± 25 % of the proton flux since the mission launch (calculated using SPENVIS [10]).

### 3.3. *The Japanese Space Agency Suzaku mission*

The Suzaku X-ray astronomical satellite was launched in July 2005. The Suzaku X-ray Imaging Spectrometers (XISs) contain three front-illuminated (FI) X-ray CCD cameras (XIS0, XIS2 and XIS3) and one back-illuminated (BI) X-ray CCD camera (XIS1). Both the FI-CCD and the BI-CCD have imaging areas of 1024×1024 with a pixel size of 24 µm × 24 µm. The depletion layers for the FI-CCD and the BI-CCD are approximately 65 µm and 42 µm respectively [11].

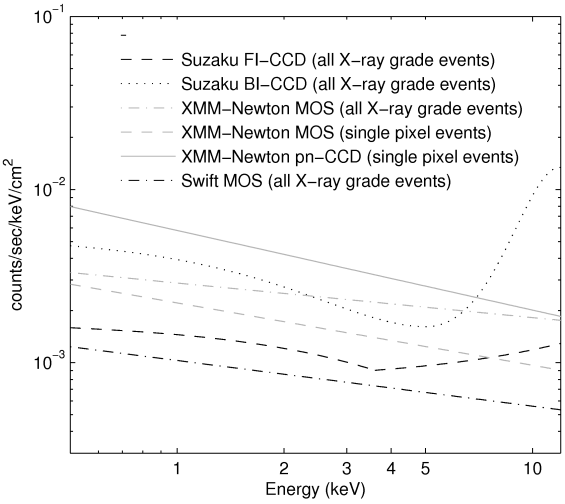


Fig. 3. The instrument background continua for all three missions, normalised to equivalent areas. References: XMM-Newton MOS (Figure 1), XMM-Newton pn-CCD [8], Swift MOS (Figure 2), Suzaku FI-CCD/BI-CCD [12].

To determine which events are to be accepted as X-ray like, the ASCA Grade system is used, splitting the events by grade type. The system defines the signal profile over a number of pixels, with grades 0, 2, 3, 4 and 6 regarded as X-ray-like [11].

The instrument background for the Suzaku CCD cameras can be measured independently from the X-ray background by looking at the night Earth. The spectra here appear more complex than those for the Swift mission which is found at a similar orbit. The comparison of the Suzaku CCD cameras with the Swift MOS camera allows the detector construction to be investigated. The spectral continua for all three missions is shown diagrammatically in Figure 3, normalised to an area of one square centimeter to allow direct comparisons to be made.

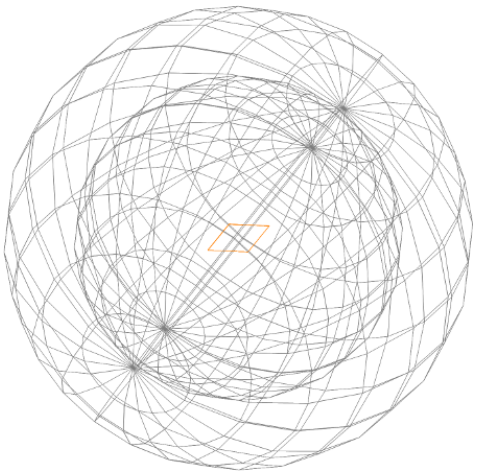

Fig. 4. A wire-mesh representation of the 3 cm thick aluminium shell used as an appropriate approximation to the detector surroundings [12]. The pixellated and layered detector sits in the centre of this shell, matching the complex construction parameters of the cameras in orbit, represented by the square shown here due to the small-scale structure of the detectors.

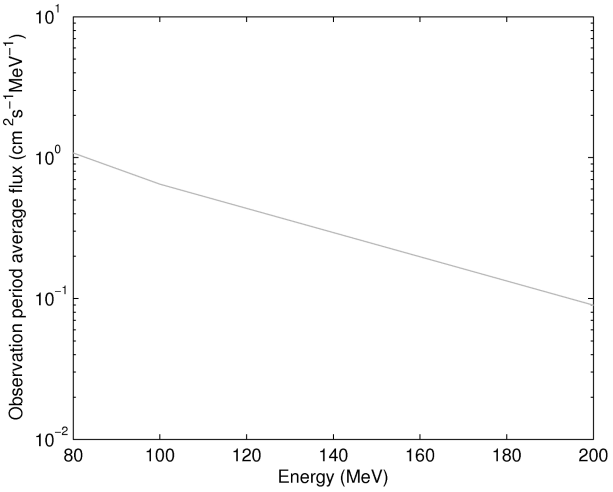


Fig. 5. The incident proton spectrum for the XMM-Newton simulation including trapped protons and a solar component averaged over the first three years in orbit (SPENVIS).

## 4. Simulation and results

The simulation was implemented using the Geant4 Monte-Carlo simulation toolkit (version 4.8.0) [13]. The range cut-offs were set to 1 µm to ensure all secondary particles were produced and tracked to within the accuracy of the detector pixelation. The passage of particles through the detectors was logged on a step-by-step basis with events combined to form the pixelated images required for analysis. Through this method, the interactions at all stages of particle transition was recorded.

The simulation geometry was based on an approximation discussed in reference [12] for the Suzaku mission. The approximation replaces the full detector surroundings with a spherical shell of thickness appropriate to the real system, Figure 4. In this way, the detector is surrounded by material which, although not of the same configuration, is of similar atomic structure and mass. Over the entire surface of the material, any variations to the real system were found not to have an adverse affect on the spectrum of particles arriving at the detector.

The detectors themselves were not approximated and appear in the simulation as they appear in orbit, only with a smaller surface area of close to 1 cm$^2$ for normalisation purposes. The geometry of the pixellated and non-pixellated layers of silicon and oxides were taken from the original detector specifications as detailed in references [3] and [4]. In the case of teh XMM-Newton pn-CCD camera, a thin copper layer was included below the device to account for the printed circuit board present.

At HEO (XMM-Newton), the proton flux was normalised to give a readout from the CCD of between 2.2 protons cm$^{-2}$ s$^{-1}$, following the spectral form shown in Figure 5 generated with SPENVIS with the appropriate mission parameters. Protons with energy lower than 70 MeV were ignored due to the low probability of passage through the aluminium shielding. The incident proton flux was modelled by a power law matching the data in Figure 5 to a maximum proton energy of 400 MeV, where the flux is two orders of magnitude lower than that at 100 MeV. The normalisation value was registered from in-orbit data in reference [14] and found to be consistent with a rate of 4.4 protons cm$^{-2}$ s$^{-1}$ in solar minimum conditions, reduced by a factor of two at solar maximum due to solar modulation. A similar study was implemented pre-launch (described in section 6) and considered the background source of Compton interactions from secondary gamma rays produced through the interaction of cosmic-rays and solar-flare protons with the detector and surroundings; other sources of background were considered insignificant [1]. This study consequently concentrates on the effect of high energy protons on the instrument background at HEO.

At LEO (Swift and Suzaku), the spectrum of incident particles was derived from references [12] and [15] and includes cosmic-ray protons, electrons and X-rays. Each particle type was tested to establish the dominant region of the energy spectrum and this region was selected for full future implementation into the simulation. The incident particle spectrum was again normalised to the proton detection rate in the detector found in orbit, giving a flux of 0.6 protons cm$^{-2}$ s$^{-1}$ at 570 km [12] for the Suzaku orbit. The normalisation was applied using the proton spectrum for Suzaku at the time of collection of the in-orbit data, Figure 6. The different inclination angles of the Swift and Suzaku orbits have little impact on the incident proton spectrum at the time of data collection, Figure 6, showing a variation of 20 % at 150 MeV and only 6 % at 300 MeV. The impact of the SAA is averaged over the orbital period of the in-orbit data collection (over twenty orbits).

The data produced in the simulation was analysed using in-house code capable of separating the various compo-

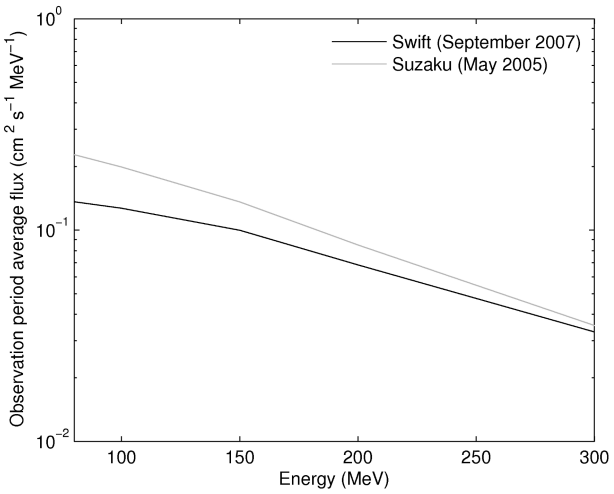


Fig. 6. The incident proton spectrum for the Suzaku mission in comparison to the Swift mission over the periods of in-orbit data collection (SPENVIS).

nents by particle (both primary and secondary), interaction type (both for the production of the interacting particle and the interaction by which energy is deposited) and the energy deposition profile. In order to concentrate purely on the components producing the instrument background continuum, fluorescence was not included. This gives a much clearer indication of the spectral form of the background and results in reduced running time for the simulation. The analysis of the results is discussed below.

The in-house code allows a full, deep analysis of the way in which the instrument background is formed. Each interaction of a particle in the detector can be tracked back to the primary incident particle. The location of the energy deposition can be tracked back through time to the initial interaction position. This allows the event to be considered as a point interaction in the silicon, such as a Compton interaction, or as a progressive energy loss such as that caused by a minimally ionising charged particle as it passes through the detector. The initial interaction position also allows the user to pinpoint where the particle entered the detector and thus examine the impact of the surface structures on the instrument background. The history of each particle can also be logged, providing an insight into how the shielding influences the spectrum of incident radiation.

Images are produced from the simulated data, Figure 7, and can be analysed in a similar way to those produced in-orbit using a grading system to select events which are deemed X-ray-like. Events classified as X-ray-like from the images can be accumulated to produce an energy spectrum. Following appropriate normalisation, the spectrum can be compared to those produced from in-orbit data, Figure 8.

## 5. Discussion

Analysis of the simulated data shows that the instrument background is built from three main components. The relative dominance of each component is dependent on not only the incident flux of particles, and hence the orbit, but also the design of the detector.

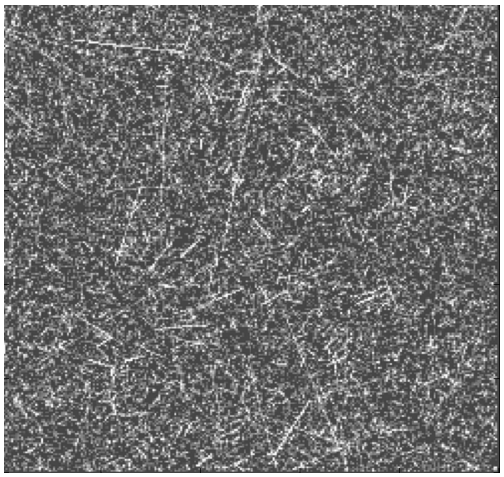

Fig. 7. A simulated image in which the tracks caused by protons passing through the detector can be seen.

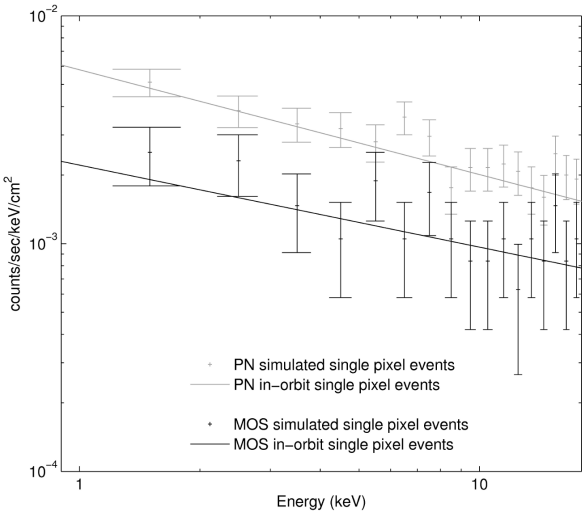


Fig. 8. The simulated instrument background for the XMM-Newton MOS and pn-CCD cameras.

### 5.1. *Compton scattering*

When a photon passes through the silicon of the detector it is possible for this photon to be Compton scattered. The probability of a high energy photon (energy greater than 100 MeV) being detected conventionally is negligible. The recoil electron is detected in the silicon as an X-ray-like event, providing it does not deposit energy over an excluded pixel pattern. Such an event is indistinguishable from an event caused by an X-ray in the energy range of interest. This component of the instrument background is more prominent in detectors with a thicker active layer due to an increased probability of interaction for the primary photon. The thicker depletion layers of the Suzaku

XIS detectors lead to a greater Compton electron component than for the MOS detector of the Swift mission due to the greater probability of interactions in the thicker layer. This can be seen in the spectra as the increase in the continuum at lower energies, Figure 3.

### 5.2. *Minimally ionising charged particle*

When a minimally ionising charged particle passes through the silicon of the detector a track of electrons is left behind. If this track crosses several pixel boundaries then the event is rejected by the grade selection. This does not exclude all cases, as it is possible for a particle to pass through the detector depositing energy in only those pixels of an accepted X-ray-like grade. For the back-illuminated devices (Suzaku XIS1 and the XMM-Newton pn-CCD) a peak in the spectrum will be seen at an energy related to the thickness of the silicon. For the pn-CCD the peak falls above the energy range of interest, but for the XIS1 detector, the peak falls at approximately 13 keV and the lower energy tail dominates the background over the upper regions of the energy region of interest. The front-illuminated devices are not fully depleted and the increased spreading of charge generated below the depleted region leads to the events being reduced by the event grading system. The reduction in the Landau peak depends on the amount of charge collected from the undepleted silicon, but nonetheless leads to a significant reduction compared to the back-illuminated devices.

### 5.3. *Knock-on electrons*

The component of most interest in this study is that caused by electrons ejected from the material surrounding the detector through ionisation, predominantly from the aluminium shell: the knock-on electrons. When a proton or electron passes through the aluminium shell it liberates electrons through ionisation along its path. The knock-on electrons are absorbed within a few micrometers of the aluminium and so only those electrons from the inner surface of the aluminium are of importance, all others are absorbed by the shielding. Similarly, the electrons which are able to reach the detector will be absorbed within a few micrometers of the surface. The energy deposited by the knock-on electrons in the simulation could be traced back to the outer surfaces of the CCDs and were found to be produced in the aluminium housing around the detector by the incident protons, Figure 9. The surface structures of each detector define how these knock-on electrons will impact the instrument background. The MOS CCDs and XIS FI-CCDs are insensitive to the knock-on electrons from the rear-face due to the thick layers of non-depleted silicon. Any surface electrode structure acts to reduce the effect of the knock-on electrons on the instrument background by absorbing some of the energy of the electrons. The absorption of some of the energy from the knock-on electrons acts to shift the spectrum to a lower energy, and due to the slope of this component of the spectrum this lowers the total instrument background. The open surface structure of the back-illuminated devices such as the XIS BI-CCD and pn-CCD increases the quantum efficiency at the expense of a greater component of instrument background from the knock-on electrons. The open structure allows all knock-on electrons to be detected and the effects of this can be seen by comparing the instrument background for the XMM-Newton MOS CCD and pn-CCD. The knock-on electrons can only be detected on the upper surface of the MOS CCD and this component is somewhat reduced, even with the open-electrode structure. For the pn-CCD, the knock-on electrons may be detected in full at the open surface and partially detected at the rear-electrode surface (not fully detected due to the copper printed circuit board). The combination of the absorption of some of the energy of the knock-on electrons and the two-sided against one-sided detector produces a large difference in the total instrument background. This effect can also be seen with the two XIS detectors types. If the Compton recoil electrons were the dominant component of the instrument background then one would expect the thicker layer of depleted silicon in the FI-CCD to give rise to a higher instrument background. This is not the case. The BI-CCD has a higher level of instrument background, explainable by the knock-on electrons.

### 5.4. *Further FI-CCD vs. BI-CCD comparison*

As a comparison with the front-illuminated devices, it is worth considering what would happen if the back-illuminated devices were mounted onto a thick silicon dummy layer. The dummy layer would reduce the knock-on electron component from the detector shielding, but any protons passing through the dummy layer would generate knock-on electrons of their own. It may be possible to reduce this new source of knock-on electrons as the proton tracks will now be in close proximity to the detected knock-on electrons, whereas protons interacting in the shielding produce knock-on electrons which can arrive at the detector independently of the proton trajectory. A dummy layer would not reduce the component of the instrument background produced by the minimally ionising charge particles as charge spreading in the dummy layer would not be detected.

The MOS FI-CCD does not only consist of the image region, but also contains a frame-store region (for frame-transfer). The frame-store region is not identical to the image region, with the main differences being namely the 'integration time', the pixel size and the structure of the electrodes. Signal will be accumulated at an average rate equal to half of that seen in the image region (ranging from zero at one end of the store to 2.4 seconds at the other). The frame-store pixels measure 12 µm × 40 µm compared to the 40 µm × 40 µm pixels in the image region. These two factors lead to a basic reduction in signal to 0.15 that

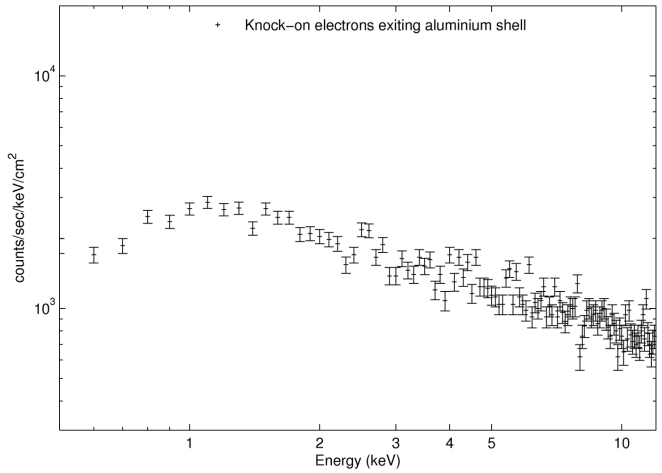


Fig. 9. The simulated spectrum of electrons emerging from the inner surface of the aluminium shell following bombardment with protons. These results were taken from the original simulation with the detector removed and all electrons emerging from the inner surface of the aluminium shell recorded.

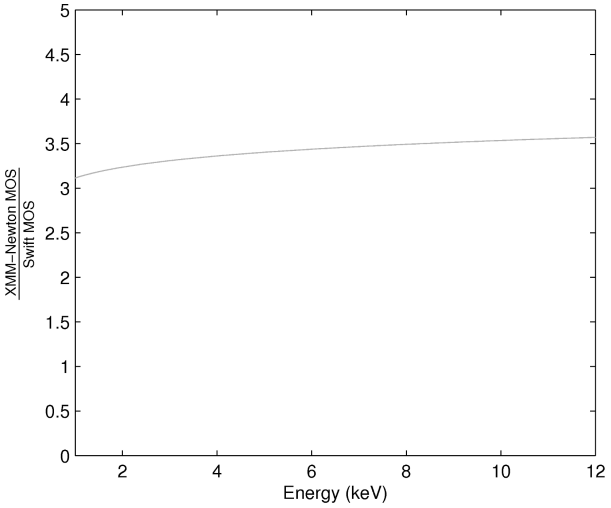


Fig. 10. The ratio between the instrument background continua for all X-ray grade events in the XMM-Newton MOS and Swift MOS spectral continua previously detailed in Figure 3.

in the image region. The electrodes in the frame-store region also follow the standard pixel construction without the open area. Combining these effects with the findings of the simulation leads to the conclusion that the instrument background accumulated in the frame-store region of the MOS FI-CCD is an order of magnitude lower than that in the image region.

### 5.5. *Orbital dependence*

The MOS camera system used in both the XMM-Newton and Swift missions allows a comparison of the effect of the orbit on the instrument background and clarification of the results previously discussed. The component of instrument background from minimally ionising charged particles is negligible as the MOS CCD is a front-illuminated device comprising of both depleted and non-depleted regions of silicon. The charge spreading in the non-depleted region causes these events to be rejected with the X-ray grading system.

If the instrument background is knock-on electron dominated, one would expect the level of background to scale predominantly with the flux of protons. It was stated previously that the flux of protons through the detector was 2-2.5 protons cm$^{-2}$ s$^{-1}$ at XMM-Newton's orbit and 0.6 protons cm$^{-2}$ s$^{-1}$ at the Swift orbit. From this ratio, taking into account the slight decrease in incident proton flux for the Swift orbit with respect to the Suzaku orbit (Figure 6), a knock-on dominated instrument background hypothesis for a similar solid angle of shielding would predict that the Swift MOS background would be approximately three to four times lower than the XMM-Newton MOS instrument background, Figure 10. This is indeed the case. The Swift MOS instrument background shares a similar form to the XMM-Newton background, but shows an increase at lower energies. At the lower orbit, with the decrease in proton flux and relative increase in photon flux, the Compton recoil electron component for the front-illuminated device is more prominent. The increase in the Swift instrument background can therefore be explained by the Compton recoil electron component.

## 6. Pre-launch predictions for XMM-Newton EPIC CCDs

Using the Integrated Radiation Transport Suite (IRTS), an ESA-funded study was completed before launch to predict the instrument background that would be experienced by the EPIC MOS CCDs on XMM-Newton in orbit [1]. The background source considered was that from Compton interactions of the secondary gamma rays produced through the interactions of cosmic-rays and solar-flare protons with the detector materials and spacecraft. The background spectra were predicted by integrating the response functions of the detectors according to the cosmic-ray and solar flare induced gamma spectrum. Following a full three-dimensional simulation, a total response for the EPIC CCDs was calculated at $3.5\times10^{-5}$ counts keV$^{-1}$ per incident proton [1].

At the incident proton rate described in reference [14] of approximately 2.2 protons cm$^{-2}$ s$^{-1}$, the pre-launch predicted instrument background continuum is approximately $7.7\times10^{-5}$ counts cm$^{-2}$ s$^{-1}$ keV$^{-1}$ with a flat spectrum. The spectral continuum found in-orbit is almost two orders of magnitude higher at 1 keV at $3\times10^{-3}$ counts cm$^{-2}$ s$^{-1}$ keV$^{-1}$.

The pre-launch study concentrated on the influence of the Compton interactions of secondary gamma rays and not the component caused by the secondary electrons (knock-on electrons). Although a Compton dominated background would show a higher count rate for the thicker pn-CCD

over the MOS CCD, the knock-on electrons were found in this study to be a dominant factor in producing the instrument background experienced in-orbit, particularly at HEO, and can also explain this difference. The flux of knock-on electrons, recorded at the CCD as simulated here, closely matches that found in-orbit and dominates over the flux of secondary gamma rays detailed in the pre-launch study by two orders of magnitude. The lower incident proton rate at LEO reduces the knock-on electron component and this reduction can be seen in the Swift MOS in-orbit instrument background. The Compton component at LEO is no longer negligible due to the differing incident spectrum and contributes to increase the instrument background above the purely knock-on electron dominated continuum at lower energies.

## 7. Sensitivity considerations

When considering the sensitivity of each camera, the instrument background must be taken into account. For the EPIC systems aboard XMM-Newton, the mirror (including the effects of the mirror on the amount of diffuse X-ray background which is resolved), filter, source and detector all need to be taken into account when considering the total sensitivity, and hence the minimum observable flux. The net effective area, found through the product of the X-ray telescope effective area and the quantum efficiency of the detector, must be combined with the background level to find the overall detector sensitivity. For the XMM-Newton EPIC MOS systems the net effective area is lower than would be expected relative to the pn-CCD system as only 44% of the telescope incident flux is directed to each of the MOS cameras, the remainder being directed to the Reflection Grating Spectrometers (RGS) and lost due to the structural obstruction by the RGS grating and supports [3]. This must be taken into account when comparing with the unobstructed beam reaching the pn-CCD camera. The differences between the quantum efficiencies of the detectors are quite significant, Figures 11 and 12, and considering the loss in effective area of over 10% with the two MOS detectors combined, the difference in sensitivity is greatly reduced due to the significantly lower instrument background for the MOS cameras.

Defining a Quality Figure (QF) for the cameras related to the signal-to-noise ratio, it is possible to examine this further. The energy range used depends on the science to be considered and will be taken at 1 keV here as an example. Assuming the mirrors and filters to be common to the two detector types, the signal can be taken as the product of the proportion of the beam reaching the detector, the QE of the device at 1 keV and the collection efficiency (CE), where the CE gives the integration to dead-time for the detector (assumed to be approximately 0.9 for the pn-CCD and 1 for the MOS). At the low signal limit, the noise can be approximated to the square root of the background, dominated by the instrument background and the cosmic X-ray background. We define the QF here as the ratio of the signal to noise as described above for each camera system.

Using background data from Figure 1 in reference [2] for the MOS background and from Figure 3 in reference [8], the relative background count rates for the MOS and pn-CCD have been extracted and normalised to the MOS instrument background. It should be noted that although the pn-CCD has approximately three times the instrument background of the MOS at 1 keV, the total background from the above data gives a slightly lower total background count-rate ratio of 9:4 at 1 keV (normalised to the XMM-Newton MOS instrument background, MOS IB = 1). These calculations are only relevant for one aspect of the science (low signal source detection) and other aspects of the science at higher energies will generate a different QF. The results of these calculations are shown in Table 1.

Table 1
The Quality Figure (QF) for the MOS and pn-CCD cameras. The QF is defined here in a similar way to the signal-to-noise ratio, but with constant factors between the systems ignored for simplicity. The 'signal' is taken as the product of the beam proportion (BP) hitting the detector, the QE and the Collection Efficiency (CE), given by the integration to dead-time ratio. The calculations are based on the low signal, background dominated case. The two MOS detectors are first examined individually (×1), then as a pair (×2). The final row shows the QF for the MOS detector if it were presented with the same unobstructed beam encountered by the pn-CCD, allowing a more direct comparison. All background levels are normalised to the XMM-Newton MOS instrument background at 1 keV.

| | BP | QE | CE | 'Signal' | Bg | QF |
|---|---|---|---|---|---|---|
| pn-CCD | 1 | 0.97 | 0.9 | 0.87 | 9 | 0.29 |
| MOS (×1) | 0.44 | 0.7 | 1 | 0.31 | 4 | 0.16 |
| MOS (×2) | 0.88 | 0.7 | 1 | 0.62 | 8 | 0.22 |
| MOS unobstructed | 1 | 0.7 | 1 | 0.7 | 7 | 0.26 |

The quality figures calculated in Table 1 show an interesting comparison between the camera systems using the front-illuminated and back-illuminated devices. If subjected to the same full beam, the difference between the quality figures for the two devices is greatly reduced, and despite the variations in device structure, within the errors of the approximations used here the devices offer equivalent performance.

The simulated data suggests that the rear of the front-illuminated devices offers better resilience to the knock-on electrons. The layers of non-depleted silicon at the rear of the devices absorb the knock-on electrons, and consequently they do not add to the instrument background count as in the case of the pn-CCD and back-illuminated devices. The front faces of the devices is where the balance must be achieved between the quantum efficiency and the level of the instrument background. A high QE device such as the pn-CCD is able to detect the lower energy photons more effectively than the MOS CCD. Unfortunately, this optimisation to the QE increases the background; as well as allowing the detection of lower energy X-rays, the knock-on electrons are also able to be fully detected. The balance

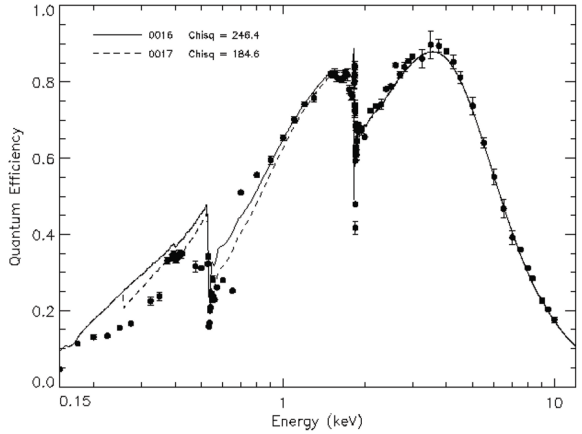


Fig. 11. The QE for the MOS CCD [17], showing a QE of 0.7 at 1 keV

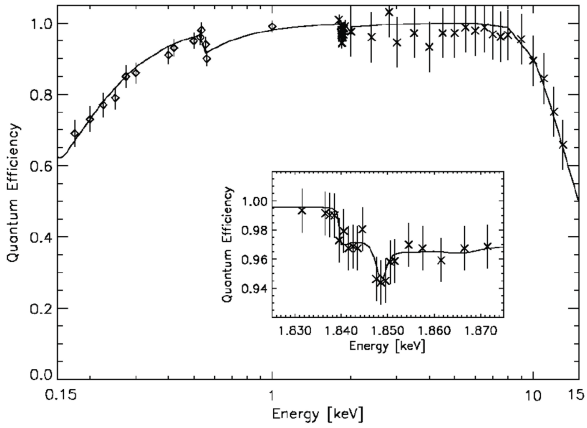


Fig. 12. The QE for the pn-CCD [17], showing a QE of 0.97 at 1 keV

between the QE and the instrument background must be carefully considered at HEO where the knock-on electron component dominates. If one is solely looking at X-rays with energies greater than 0.5 keV then a back-illuminated structure (particularly one which is able to detect knock-on electrons from both major faces) is not necessarily ideal from a sensitivity perspective, although the QE at lower energies may appear more desirable. The QE at higher energies ($> 4$ keV) for front-illuminated detectors (similar to the MOS) has improved dramatically over the last decade and should no longer be a deciding factor in detector choice [16].

## 8. Conclusions

Previous studies based on Compton interactions from secondary gamma rays under-predict the instrument background at HEO. The simulation carried out here shows the dominating component of the background at HEO is caused by the knock-on electrons produced by the passage of protons through the detector shielding. The influence of the knock-on electrons is greatly affected by the design of the device, with the surface structure defining how the electrons will be detected. It is worth, therefore, not only considering the effect of the structure of the device on the quantum efficiency of the system but also the influence the structure will have on the instrument background. The possibilities of using a graded-shield for the innermost camera layers could be explored in future work to assist in reducing the instrument background from knock-on electrons and may help reduce fluorescence [18]. Any considerations to reduce the instrument background must be carefully balanced with their effect on the X-ray fluorescence peaks. Through these considerations the sensitivity of future camera systems can be optimised.

## Acknowledgements

With thanks to Andrew Read, University of Leicester, and Claudio Pagani, Penn State University, for their help in providing the in-orbit spectral data and with thanks to Martin Turner, University of Leicester for his general advice and discussion at the outset of this work. Also with thanks to Jason Gow, The Open University, for his advice on the use of SPENVIS.

## References

[1] C. S. Dyer, P. R. Truscott, H. E. Evans, C. L. Peerless, IEEE Transactions on Nuclear Science, 43 6 (1996).
[2] De Luca, S. Molendi, Proc. Symposium 'New Visions of the X-ray Universe in the XMM-Newton and Chandra Era' (2001).
[3] M. J. L. Turner, et al., A&A 365 (2001) L27-L35.
[4] L. Strüder, U. Briel, K. Dennerl, et al., A&A 365 (2001) L18-L26.
[5] A.M. Read, T.J. Ponman, A&A 409 (2003) 395-410.
[6] http://xmm.esac.esa.int
[7] J. U. Ness, M. Ehle, R. González Riestra, M. Guainazzi, P. Rodríguez, A. Talavera, I. de la Calle, XMM-Newton Users Handbook, Issue 2.7 (17.09.2009).
[8] M. J. Freyberg, U. G. Briel, K. Dennerl, F. Haberl, G. Hartner, E. Pfeffermann, E. Kendziorra, M. Kirsch, D. Lumb, Proceedings of SPIE Volume 5165, X-Ray and Gamma-Ray Instrumentation for Astronomy XIII (2004).
[9] N. Gehrels, G. Chincarini, et al., Astrophys.J. 611 (2004) 1005-1020.
[10] D. Heynderickx, B.Quaghebeur, E. Speelman, and E.Daly, AIAA-2000-0371 (2000).
[11] K. Koyama, H. Tsunemi, T. Dotani et al., PASJ 59 (2007) S23-S33.
[12] H. Murakami, M. Kitsunezuka, M. Ozaki, T. Dotani and T. Anada, Proceedings Vol. 6266, Space Telescopes and Instrumentation II: Ultraviolet to Gamma Ray, 62662Y (2006).
[13] S. Agnostelli, J. Allison, K. Amako, et al., NIM A 506 3 (2003) 250-303.
[14] D. H. Lumb, R. S. Warwick, M. Page, and A. De De Luca, A&A 389 (2002) 93-105.
[15] T. Mizuno, T. Kamae, G. Godfrey, T. Handa, D. J. Thompson, D. Lauben, Y. Fukazawa, and M. Ozaki, Astrophysical Journal 614 (2004) 1113-1123.
[16] N. J. Murray, A. D. Holland, D. R. Smith, J. P. Gow, P. J. Pool, D. J. Burt, NIM A 604 (2008) 180-182.
[17] M. Guainazzi et al., EPIC status of calibration and data analysis, XMM-SOC-CAL-TN-0018-2-7-1 (2008).
[18] E. Pfefferman, P. Friedrich, M. Freyberg, G. Kettenring, L. Krämer, N. Meidinger, P. Predehl, L. Strüder, High-Energy Detectors in Astronomy 5501 (2004).